The 2018 reawakening and eruption dynamics of Steamboat Geyser, the world's tallest active geyser

Mara H. Reed[a,1], Carolina Munoz-Saez[b,c], Sahand Hajimirza[d], Sin-Mei Wu[e], Anna Barth[c], Társilo Girona[f], Majid Rasht-Behesht[g], Erin B. White[h], Marianne S. Karplus[i], Shaul Hurwitz[j], and Michael Manga[a,1]

[a]Department of Earth and Planetary Science, University of California, Berkeley, CA 94720; [b]Department of Geology, Universidad de Chile, Santiago, Chile 8320000; [c]Lamont–Doherty Earth Observatory, Columbia University, New York, NY 10027; [d]Department of Earth, Environmental and Planetary Sciences, Rice University, Houston, TX 77005; [e]Department of Geology and Geophysics, University of Utah, Salt Lake City, UT 84112; [f]Geophysical Institute, University of Alaska Fairbanks, Fairbanks, AK 99775; [g]Department of Earth, Environmental, and Planetary Sciences, Brown University, Providence, RI 02912; [h]Yellowstone National Park, National Park Service, Mammoth, WY 82190; [i]Department of Geological Sciences, University of Texas at El Paso, El Paso, TX 79968; and [j]Volcano Science Center, US Geological Survey, Moffett Field, CA 94035

This contribution is part of the special series of Inaugural Articles by members of the National Academy of Sciences elected in 2018.

Contributed by Michael Manga, November 18, 2020 (sent for review October 8, 2020; reviewed by Einat Lev and Thomas R. Walter)

Steamboat Geyser in Yellowstone National Park's Norris Geyser Basin began a prolific sequence of eruptions in March 2018 after 34 y of sporadic activity. We analyze a wide range of datasets to explore triggering mechanisms for Steamboat's reactivation and controls on eruption intervals and height. Prior to Steamboat's renewed activity, Norris Geyser Basin experienced uplift, a slight increase in radiant temperature, and increased regional seismicity, which may indicate that magmatic processes promoted reactivation. However, because the geothermal reservoir temperature did not change, no other dormant geysers became active, and previous periods with greater seismic moment release did not reawaken Steamboat, the reason for reactivation remains ambiguous. Eruption intervals since 2018 (3.16 to 35.45 d) modulate seasonally, with shorter intervals in the summer. Abnormally long intervals coincide with weakening of a shallow seismic source in the geyser basin's hydrothermal system. We find no relation between interval and erupted volume, implying unsteady heat and mass discharge. Finally, using data from geysers worldwide, we find a correlation between eruption height and inferred depth to the shallow reservoir supplying water to eruptions. Steamboat is taller because water is stored deeper there than at other geysers, and, hence, more energy is available to power the eruptions.

Yellowstone | Steamboat | geyser | hydrothermal | seasonality

On 15 March 2018, Steamboat Geyser in Yellowstone National Park's Norris Geyser Basin (Fig. 1; refs. 1, 2) had its first major eruption following a 3.5-y dormancy. Since then, Steamboat has erupted 109 times as of 31 July 2020—already a greater number than any previous active phase on record (Fig. 2). Its eruption plumes can reach heights that exceed 115 m (2, 3), which is currently taller than any other geyser worldwide. Steamboat's new active phase, thus, drew significant public attention and widespread press coverage. The renewed eruptions highlighted some fundamental open questions about intermittent natural processes that result from localized input of energy and mass and, more specifically, on geyser dynamics (4):

Why did Steamboat become active again?

What processes or thermodynamic conditions control the interval between its eruptions?

Why are Steamboat's eruptions tall compared to other geysers'?

Major eruptions of Steamboat may be a manifestation of deeper magmatic processes. Wicks et al. (5) proposed that renewed eruptions at Steamboat resulted from uplift episodes of Norris Geyser Basin from 2013 to 2014 and again since 2016. The inflation was attributed to magma intrusion in the late 1990s and ascent of magmatic volatiles to shallow depths (5). If this interpretation of geodetic data is correct, the questions listed are not just related to geysers, but are also connected to larger-scale magmatic processes and volcanic hazards, possibly including hydrothermal explosions, such as those that have occurred in Norris Geyser Basin (2, 6).

Here, we first provide an overview of Steamboat Geyser's geologic setting, physical characteristics, and eruptive behavior, and then address the three outlined questions with a combination of observations and models. We use seismic, ground-deformation, hydrologic, geochemical, and satellite-based thermal infrared data to look for changes correlated with Steamboat's reactivation. To determine what influences its eruption intervals, we search for empirical relations among intervals and ejected water volumes, meteorological data, ground deformation, and seismicity. Last, we use chemical geothermometry (7) and the thermodynamic properties of eruptions to identify controls on eruption heights.

Steamboat Geyser

Geologic Setting. Steamboat Geyser is in Norris Geyser Basin (Fig. 1), which is adjacent to the northern rim of the 0.631-million-year-old Yellowstone Caldera (8, 9) and the southern end of the Norris-Mammoth Corridor, a structure containing postcaldera rhyolitic domes and basaltic lava vents (2, 9). The geyser basin is also located at the easternmost extent of the

Significance

Natural geysers episodically erupt liquid water and steam and, thus, provide a window into multiphase hydrothermal systems. The size of and interval between eruptions can shift over time due to changes in the hydrothermal system and due to deeper magmatic processes. An improved understanding of geyser dynamics can provide insights into other multiphase episodic processes on Earth and other planets that result from localized input of energy and mass (e.g., volcanism).

Author contributions: S. Hurwitz and M.M. designed research; M.H.R., C.M.-S., S. Hajimirza, S.-M.W., T.G., E.B.W., S. Hurwitz, and M.M. performed research; M.H.R., C.M.-S., S.-M.W., A.B., T.G., M.R.-B., E.B.W., M.S.K., and S. Hurwitz analyzed data; and M.H.R., C.M.-S., S. Hajimirza, S.-M.W., A.B., T.G., M.S.K., S. Hurwitz, and M.M. wrote the paper.

Reviewers: E.L., Columbia University; and T.R.W., Helmholtz Centre Potsdam–GFZ German Research Centre for Geosciences.

The authors declare no competing interest.

[1]To whom correspondence may be addressed. Email: reed.mara.h@gmail.com or manga@seismo.berkeley.edu.

This article contains supporting information online at https://www.pnas.org/lookup/suppl/doi:10.1073/pnas.2020943118/-/DCSupplemental.

Published January 4, 2021.

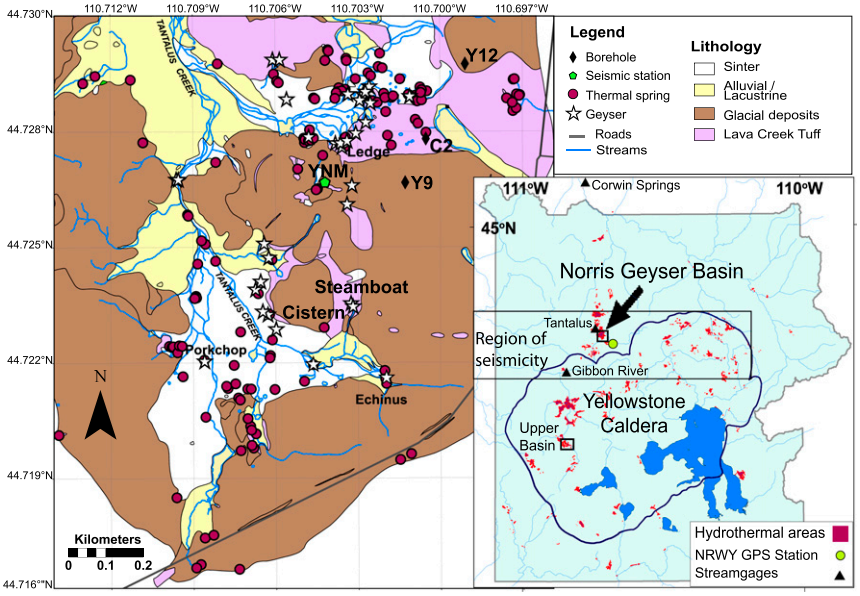

Fig. 1. Geologic map of Norris Geyser Basin and its surrounding area (after refs. 1, 2). Locations of key geysers, thermal springs, streams, seismic station YNM, and boreholes Y12, C2, and Y9 are shown on the map. *Inset* map shows the location of Norris Geyser Basin relative to the Yellowstone Caldera, boundaries of Yellowstone National Park, GPS station NRWY, relevant USGS streamgages, and the region of seismicity analyzed in this work.

Hebgen Lake fault system, which accounted for 75% of the Yellowstone region's earthquakes between 1973 and 2006 (10). The 1959 moment magnitude (M_w) 7.3 Hebgen Lake, Montana earthquake was about 50 km west-northwest of Norris Geyser Basin, and both of the largest earthquakes in the Yellowstone Plateau in the last 50 y, the local magnitude (M_L) 6.1 in 1975 (11) and the M_w 4.8 in 2014, had epicenters within 8 km of the geyser basin.

The bedrock in Norris Geyser Basin consists of the Lava Creek Tuff, which erupted when the Yellowstone Caldera was formed. This ∼300-m-thick unit consists of densely welded ash divided into subgroups A and B (9). The contact between them is a relatively permeable zone occurring at a depth of ∼40 m (2). Throughout most of the geyser basin, the Lava Creek Tuff is covered by siliceous sinter, glacial, and alluvial/lacustrine deposits (Fig. 1). The basin's hydrothermal system is notable for its diverse water chemistry and the hottest temperatures recorded in Yellowstone at a subaerial vent (138 °C in a fumarole; ref. 12) and during research drilling (237 °C at a depth of 331 m in borehole Y12; ref. 13).

Unlike cone-type geysers in Yellowstone's Upper Geyser Basin (Fig. 1) that have existed for thousands of years (14, 15), such as Old Faithful, Giant, and Castle Geysers, Steamboat is probably a relatively young geyser that broke out or significantly enlarged itself in August 1878 "with such upturning and hurling of rocks and trees" (ref. 16, p. 16). Since then, the geyser's powerful eruptions have eroded sediment and discouraged tree growth in a 15- to 30-m radius. Present-day Steamboat Geyser consists of two vents (often referred to as the North and South Vents) in the middle of an open hillside strewn with boulders and rock fragments (Fig. 3*A*). Thin sinter deposits exist in and around the vents and along the geyser's major runoff channels; the rest of the exposed rock is altered Lava Creek Tuff (2).

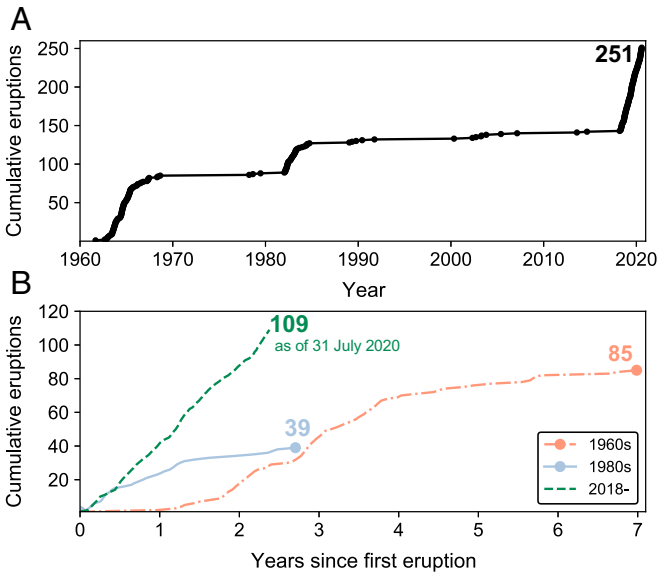

Fig. 2. Steamboat's major eruptions in the GeyserTimes database as of 31 July 2020, excluding one eruption in 1911. We note that this database undercounts eruptions in the 1960s and differs from the yearly counts published in White et al. (2); see *Eruption Datasets* for details. (*A*) Cumulative eruptions since 1961, prior to which there was a 50-y dormancy. Most eruptions occur during active phases. (*B*) Comparative progression of the three active phases. We define the eruptions on 2 September 1961, 13 January 1982, and 15 March 2018 as the beginning of the 1960s, 1980s, and late-2010s active phases, respectively.

Steamboat Eruption Dynamics. Steamboat has two eruption styles. Minor eruptions, also called preplay, range from wispy, angled jetting to vertical surges up to 15 m from one or both vents (2). Major eruptions begin like minor eruptions, but, instead, become progressively taller and more violent. Some major eruptions in the 1960s reached maximum heights of 83 to 116 m, based on triangulation from photographs (3, 17). Because the North Vent's jet is taller, the water column appears lopsided (Fig. 3*B*). Major eruptions end with a roaring steam phase that slowly diminishes over many hours (2, 18), but the boundary between liquid and steam phases is ambiguous. Many, but not all, eruptions involve short-lived steam phases that transition back to liquid and vice versa, periods with one vent in steam phase while the other vent is in liquid phase, and/or abrupt pauses in emissions from both vents (19). The main liquid phase lasts for a duration of 3 to 90 min, but the exact definition of duration varies between observers due to this ambiguity (19). Following the end of the final steam phase, Steamboat discharges no water until minor eruptions resume several days later.

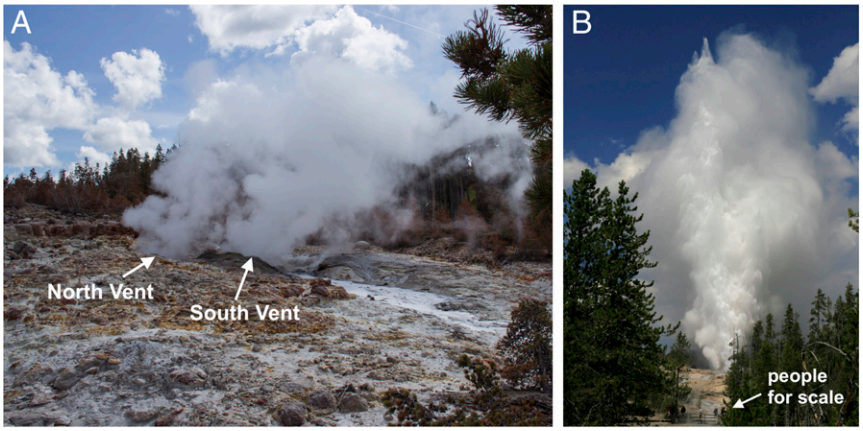

Fig. 3. (*A*) Steamboat's crater on 30 May 2019 showing the locations of its two vents and the disturbed area around them. The runoff channel is coated in fresh, white sinter. Photo in *A* is from the authors. (*B*) A major eruption on 4 August 2018 reaching full height. Note that the people in the bottom center of the frame are ∼65 m away from the geyser. Image credit: Bruce H. Jensen (photographer).

Steamboat's eruption intervals, the periods between major eruption start times, range from 3 d to 50 y based on available records (2, 19). Prior to modern electronic monitoring, records come from visitor and National Park Service personnel observations that were published in reports and local newspapers. Steamboat alternates between active phases, which we define as a prolonged series of major eruptions with a majority of intervals lasting from days to weeks, and relatively dormant periods punctuated only by isolated major eruptions (Fig. 2*A*). We identify three active phases (Fig. 2*B*): 1) between early September 1961 and early 1969, 2) between 13 January 1982 and 26 September 1984, and 3) since 15 March 2018. Minor eruptions commonly occur through both active phases and dormancies (2, 18). In fact, after viewing the aftermath of the 1961 major eruption (likely the first since 1911), one observer expressed concern that "one of the prettiest small geysers of Yellowstone" had damaged itself and might not return to "normal" (20). Henceforth, the term "eruption" when used in the context of Steamboat refers to its major eruptions, and the term "interval" refers to the interval before the eruption in question.

Cistern Spring, located ∼100 m to the southwest (Fig. 1), is the only thermal feature with documented evidence for a subsurface hydraulic connection to Steamboat. The pool was full of gray, boiling water in the early 1950s (18). Sometime between the late 1950s and mid-1960s, it became a brilliant turquoise color and discharged enough water downslope to kill nearby trees (2, 21). In the summer of 1966, Cistern's water level began draining several meters after every major eruption of Steamboat (2). This relationship continues into the current active phase (22).

Why Did Steamboat Become Active in 2018?

Dormant geysers elsewhere have resumed frequent eruptions following large earthquakes (23), the cessation of geothermal development (e.g., ref. 24), and other human interventions such as soaping (25) and drilling (26). Here, we search for triggering mechanisms to explain Steamboat's active phases. Owing to improvements in monitoring data availability and quality in Yellowstone, we focus on the latest active phase and explore variations in geophysical and geochemical parameters prior to Steamboat's reactivation in 2018. We first consider annual precipitation (rain and snowfall) and seismicity, two external factors that are known to affect geyser activity (27–29). Then, we investigate processes related to uplift episodes in Norris Geyser Basin: ground deformation (5), radiant heat emissions, and changes in the geothermal reservoir temperature.

Precipitation. Meteoric water recharge into deep geothermal reservoirs can affect geyser-eruption intervals at annual to decadal timescales (28). The loss of recharge due to decades of dry climate can even lead to eruption cessation (15). We, thus, search for correlation between the number of Steamboat Geyser eruptions per year between 1960 and 2019 and the mean annual water discharge in the Yellowstone River at Corwin Springs, Montana (Fig. 1, *Inset*), which we use as a proxy for total annual precipitation in Norris Geyser Basin (*SI Appendix*, Fig. S1). Overall, we find no pattern and conclude that higher annual precipitation rates were likely not the cause of eruption reactivation.

Seismicity. A host of observations and laboratory experiments have shown that the dynamic stress from distant and regional earthquakes can change permeability and, hence, fluid flow in the crust (e.g., ref. 30). Dynamic stresses on the order of $>10^{-1}$ MPa have changed the eruption intervals of Daisy and Old Faithful Geysers in Yellowstone's Upper Geyser Basin (27, 29). A dynamic stress of 10^{-1} MPa corresponds to a peak ground velocity (PGV) of 10^{-2} m/s, similar to the minimum ground velocity that results in other hydrological responses (31).

Earthquake swarms around the northern Yellowstone Caldera rim in June–August 2017 and February 2018 preceded Steamboat's reactivation (Fig. 4). These earthquakes, part of the Maple Creek sequence, were interpreted both as a swarm driven by magmatic fluids (32) and as aftershocks from the 1959 M_w 7.3 Hebgen Lake, Montana earthquake (33). We calculated PGV at seismic station YNM in Norris Geyser Basin (Fig. 1) resulting from both local and teleseismic earthquakes since mid-2013 (*SI Appendix*, Figs. S2 and S3). During the Maple Creek sequence, PGV in Norris Geyser Basin remained below the threshold of 10^{-2} m/s found to affect geyser eruptions elsewhere. We conclude that it is highly unlikely that the Maple Creek sequence caused Steamboat's 2018 reactivation. The only time PGV exceeded 10^{-2} m/s was in response to a M_w 4.8 earthquake on 30 March 2014 located ∼5 km east-northeast of Steamboat. The geyser erupted 5 mo later on 3 September 2014, but, given the time lag, it is unlikely that the earthquake caused this eruption.

Ground Deformation and Thermal Anomalies. We examined the inference that recent deformation episodes centered around Norris Geyser Basin, caused by progressive ascent and accumulation of magmatic volatiles in the shallow brittle crust, led to Steamboat's 2018 reactivation (5). If deformation is related to the ascent of deeper and hotter fluids, we might expect to see a temperature increase in the hydrothermal system. Thermal infrared imagery acquired from survey flights (34, 35) and satellites (36) has been used to monitor changes in heat flow and thermal manifestations in Norris Geyser Basin. We analyzed Moderate Resolution Imaging Spectroradiometer (MODIS) satellite data to infer the temporal variation of median radiant thermal anomaly. We considered a 4-km^2 area centered on Norris Geyser

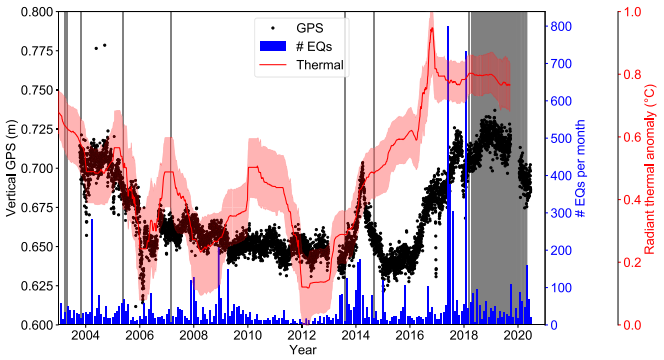

Fig. 4. Time series of different geophysical observations. We show vertical ground deformation (black) in Norris Geyser Basin measured at station NRWY, long-term radiant thermal anomaly (red, with 95% CI) of a 2 × 2-km^2 area centered at Norris Geyser Basin compared to a reference area without hydrothermal activity, and monthly earthquake (EQ) counts (blue) around the northern border of the caldera (open rectangle in Fig. 1). Vertical lines (gray) identify the eruptions of Steamboat since mid-2003.

Basin in reference to an area outside of Yellowstone National Park and without surface hydrothermal features (*Thermal Emissions*). On the timescale of several years, deformation and radiant heat emissions undulated with an overall decreasing trend from 2003 to 2012 (Fig. 4). Median radiant temperature increased ∼0.8 °C starting in 2013 and leveled out in 2017–2018; interestingly, this rate of increase remained the same during a time of rapid inflation and deflation punctuated by the M_w 4.8 earthquake in 2014. The uplift episode preceding Steamboat's reactivation did not begin until 2016. Although the small, early 2017 spike in radiant heat emissions may be an artifact because short-term trends (<6 mo) are less reliable due to the filtering method applied to the data, it is coincident with sharp deflation (∼5 cm) of Norris Geyser Basin.

To complement our analysis of radiant heat emissions, we looked for temperature variations in Steamboat's geothermal reservoir. There is precedent for increasing reservoir temperature occurring alongside more vigorous geyser activity. Based on chemical geothermometry (7), it was inferred that the geothermal reservoir temperature of Porkchop Geyser (430 m from Steamboat; Fig. 1) increased by 60 to 70 °C starting in 1962; eruptions began in 1971 and became progressively more violent and frequent until a small hydrothermal explosion in 1989 (6). To look for similar changes in the deep reservoir supplying water to Steamboat, we calculated reservoir temperatures using long-term geochemical data from samples collected at Cistern Spring (hydraulically linked to Steamboat; refs. 2, 22) and the iGeoT Multireaction Equilibrium Geothermometry (MEG) code (37). Within the ±15 °C accuracy of the method (38), there were no significant variations in reservoir temperature between 2000 and 2019 (Fig. 5). The small fluctuations were slightly less than the magnitude of seasonal variations in reservoir temperature based on multiple samples collected at Cistern Spring in 1995 (39).

Discussion of Triggering Mechanisms. Our results suggest that Steamboat's 2018 reactivation was not triggered by external factors, such as varying water recharge or dynamic stresses associated with earthquakes, but, rather, by internal hydrothermal processes. If inflation reflects the progressive supply and accumulation of hot magmatic volatiles in the shallow, brittle crust beneath Norris Geyser Basin (5), then the associated stresses, increased pore fluid pressure, and supply of enthalpy to the geothermal reservoir could potentially trigger Steamboat eruptions. Trends in thermal emissions and ground deformation are, in fact, similar on multiyear timescales. The ∼0.8 °C increase in median radiant temperature anomaly is similar to that observed prior to some volcanic eruptions (40).

We argue, however, that the available data are ultimately insufficient to relate Steamboat's reactivation to uplift episodes at Norris Geyser Basin. The roughly constant reservoir temperature calculated for Cistern Spring does not indicate anomalous subsurface changes. Missing are other indicators that the deformation affected the hydrothermal system. There was no anomalous increase in hydrothermally derived chloride or sulfate flux in the Gibbon River, which primarily originate from Norris Geyser Basin (41) (*SI Appendix*, Fig. S4). Ledge and Echinus, two of the geyser basin's significant geysers, did not reactivate at the same time as Steamboat, though Echinus experienced a short-lived active phase in late 2017 (42). Out of a small sample of seven other geysers within the Yellowstone Caldera chosen for their relatively complete records, none have active periods that correlate with caldera uplift between 1996–2020 (*SI Appendix*, Fig. S5).

Steamboat's reactivation may arise from processes that operate purely within its local hydrothermal system. Geyser activity is highly dependent on permeability of the conduit and surrounding rock matrix (43). Slow changes in temperature, pressure, and solution composition affect amorphous silica (opal) precipitation and dissolution kinetics in hydrothermal systems (e.g., refs. 44, 45), which, in turn, alters permeability. Future models and experiments involving geophysical monitoring of the subsurface and geochemical monitoring of erupted water might provide more insights into the conditions that create episodic active–dormant transitions in geysers.

What Controls the Interval between Eruptions?

Geyser-eruption intervals are primarily controlled by internal processes and subsurface structure (4), but they may also be sensitive to seasonal hydrologic processes (28), weather conditions (wind speed, air temperature, and atmospheric pressure; refs. 29, 46, and 47), earthquakes (23, 27, 29), and subsurface connections to other thermal features (46–49). Limited attention has been given to Steamboat's eruption intervals within active phases. There are observations of longer intervals at Steamboat during periods when Norris Geyser Basin was characterized by increased boiling and turbidity in springs, changes in water chemistry, and irregular geyser activity, most commonly during the summer or early fall (2, 18). It was proposed that these variations occur in response to lower pressures within the hydrothermal system (39). Here, we report a summary of

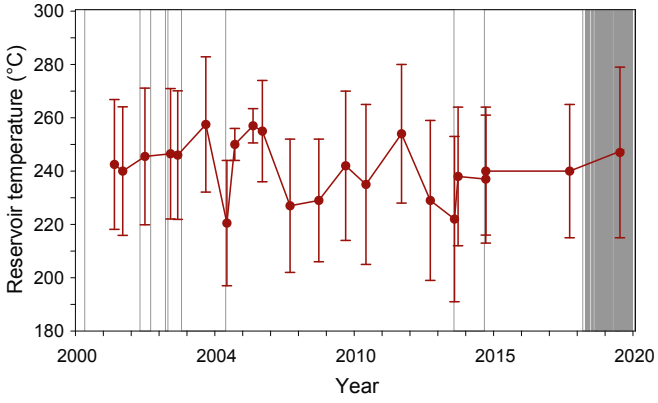

Fig. 5. Reservoir temperature for Cistern Spring waters (red markers) based on thermodynamic calculations using the iGeoT MEG code (37). Error bars represent the calculated SD and estimated accuracy of the temperatures (38). Vertical gray lines show dates of Steamboat eruptions. Leading up to the current Steamboat phase, the reservoir temperature remained roughly constant.

Steamboat's eruption intervals during the latest active phase and consider possible influences on the intervals.

Seasonality and Outlier Intervals. The median interval for the 108 eruptions between April 2018 and July 2020 is 7.17 d, in a range of 3.16 to 35.45 d. Most (86%) of the intervals are under 10 d (Fig. 6*A*). There appears to be an annual modulation of eruption intervals, with longer intervals in the winter months and shorter intervals during the summer. However, there are notable exceptions. April and August are months with higher median intervals than would be expected from the seasonal variation, and their intervals vary more widely than in other months. Intervals do not correlate with wind speed or air pressure at the time of eruption.

We count the monthly number of Steamboat eruptions and compare them to monthly mean discharge in the Gibbon River (Fig. 1), which drains Norris Geyser Basin and serves as a proxy for regional precipitation. During the latest active phase, we observed a peak in the number of eruptions each year during the late spring (May) through the midsummer (July), coincident with the increase in river discharge following snowmelt (Fig. 6*B*). We found a temporal cross-correlation coefficient of 0.23, suggesting a possible direct connection to seasonal hydrologic processes. Lags of 1 to 3 mo produced weaker correlations.

We evaluated seismic spectral-amplitude measurements (SSAMs) from station YNM (Fig. 1) in search of temporal correlations with Steamboat's intervals and the seismic signals from underlying hydrothermal systems. Here, we focused on the 0.8- to 1.2-Hz SSAM band (Fig. 7) that is commonly observed in active hydrothermal areas (e.g., ref. 50). The SSAM showed a sharp ~50% reduction after Steamboat's reactivation in March 2018, which was followed by the longest interval in the active phase (35.45 d); a similarly abrupt, but smaller, decrease occurred in late March 2019, followed by two long intervals. The largest decrease after the SSAM peak in late June 2018 also occurred before four abnormally long intervals. We note that the June 2018 peak was coincident with basin-wide anomalous activity (51), similar in some ways to that associated with longer Steamboat eruption intervals during the active phase in the 1980s (2). The reductions in SSAM do not temporally correlate with ground deformation, which implies that the seismic source is shallow and local, perhaps from within the Norris hydrothermal system. Although station coverage does not allow us to determine source locations, the decrease in SSAM is from a weakening of the source, rather than changes in source frequency (*SI Appendix*, Fig. S6). It is not possible to determine whether this weakening could be a cause or effect of longer eruption intervals, or whether both changes occur due to a yet-unidentified subsurface process.

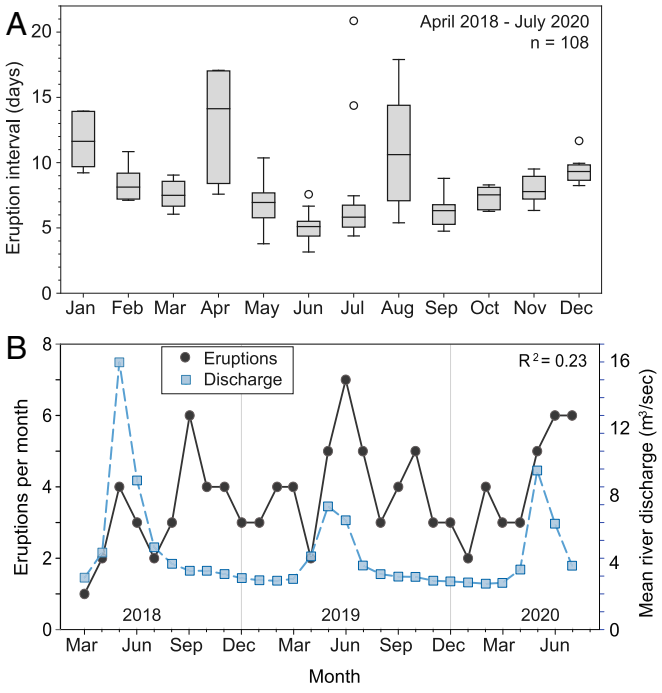

Fig. 6. (*A*) A boxplot of eruption intervals during the most recent active phase (excluding the first 3.5-y interval) binned by common month. Boxes are drawn between the first and third quartiles of data with a black line representing the median. The whiskers extend outward to the closest value within 1.5(*Q*3 − *Q*1). Outliers are plotted as open circles; a 35.45-d outlier (19 April 2018) is not shown. Overall, the median interval shows a seasonal trend, except for the months of April and August, when intervals are most variable. The July outliers both occurred in 2018. (*B*) Number of eruptions per month between March 2018 and July 2020 (dark gray line) and the monthly average discharge of the Gibbon River (USGS streamgage 06037100; dashed blue line).

Erupted Volume. For a constant input of heat and water, it might be reasonably expected that eruption intervals correlate with the volume of water ejected during individual eruptions. For both a laboratory model and a geysering well in Calistoga, California, a relationship was found between the eruption duration (a proxy for erupted volume) and the following interval between eruptions, but the distribution of durations in a series of eruptions was stochastic (52). Similarly, intervals of Old Faithful depend on the duration of the previous eruption (53). At Strokkur Geyser in Iceland, eruptions consist of one to six discrete bubble bursts; longer intervals follow eruptions with more bursts, but the burst count and seismic amplitude of individual eruptions cannot be predicted (54).

We used stream-discharge measurements from Tantalus Creek within Norris Geyser Basin (Fig. 1) to estimate Steamboat eruption volumes. For the 59 eruptions with available meteorological data and appropriate streamflow conditions for volume estimation, we found a negative correlation between wind speed and the volume of water discharged (Fig. 8*A*). This implies that stronger winds divert some erupted water away from established runoff channels. Thus, for erupted volume calculations, we considered only 29 eruptions that occurred when wind speeds were ≤1 m/s (*SI Appendix*, Fig. S7). The volumes range from 134 to 538 m^3 with a median of 351 m^3. For comparison, also using Tantalus Creek discharge data, Friedman (55) estimated Steamboat eruption volumes of 215 m^3 (2 May 2000), 130 m^3 (26 April 2002), and 246 m^3 (13 September 2002). We found no relation between erupted volume and the interval before or after the eruption (Fig. 8 *B* and *C*), implying unsteady heat and mass flow at Steamboat. We also found no relation between eruption volume and air temperature, air pressure, or amplitude of ground motion (*SI Appendix*, Fig. S8). Correlation coefficients between eruption volume and other parameters are tabulated in *SI Appendix*, Table S1. Our results are limited due to the small sample size, and we emphasize that the calculated volumes should be considered as minimum estimates of ejected liquid-water volume.

Why Are Steamboat Eruptions so Tall?

Steamboat's eruptions reach heights that exceed 115 m (2, 3), the highest of presently active geysers. We tested two hypotheses about why Steamboat reaches such lofty heights: 1) Its deep geothermal reservoir, where water and rocks equilibrate chemically, is hotter than those connected to other geysers; or 2) the shallow source that directly feeds Steamboat's eruptions is deeper than at other geysers. Hereafter, we use "reservoir" to refer to the deep geothermal reservoir and "water source" to refer to the shallow subsurface void or cavity ("bubble trap"; ref. 56) where water is stored prior to the eruption. Understanding

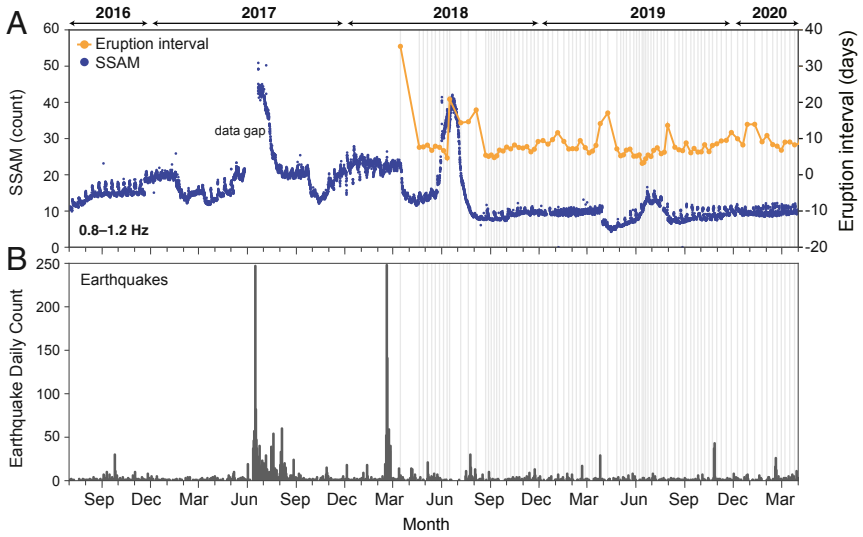

Fig. 7. (*A*) SSAM (blue dots) for 0.8 to 1.2 Hz at YNM from June 2016 to April 2020. The orange line shows the intervals following the eruptions marked by the vertical gray lines. Abrupt decreases in SSAM occur around the same time as anomalously long intervals. (*B*) Daily count of local earthquakes (dark gray bars) occurring within the box shown in Fig. 1 in comparison to Steamboat's eruptions (light gray lines).

why Steamboat's eruptions are so tall addresses a fundamental question about geysers: What controls their eruption height?

To evaluate whether a hotter reservoir temperature is correlated with the height of geyser eruptions, we considered the chemical composition of 14 different geyser waters from around Yellowstone. The reported heights for geysers other than Steamboat range from 2 m for Pearl to 84 m for Giant (18). The equilibrium reservoir temperature calculated with the iGeoT MEG code (37) is not correlated with eruption height (Fig. 9*A*).

A compilation of water source (bubble trap) depths from geysers worldwide suggests that Steamboat's water source (20 to 27 m; ref. 22) is the deepest, and its eruption column is the highest (Fig. 9*B*). We highlight that there are large uncertainties in water-source depth. Determining the existence and depth of shallow reservoirs is fraught with challenges, since the shallow subsurface is highly heterogeneous at various spatial scales. Water-source depth is inferred with multiple techniques. Direct observations define shallow sources as bends in the conduit passing from vertical to horizontal for Velikan, Bol'shoy, Kovarny, and Vanna in Kamchatka, Russia (56) or significant changes in conduit geometry for Strokkur, Iceland (57). Changes in thermodynamic conditions inside the conduit, such as a sharp increase in temperature with depth, have been interpreted as shallow water sources for Vega Rinconada in El Tatio, Chile (49) and Strokkur (57). Seismic surveys have provided useful insights about source dimensions and depth at Lone Star (58, 59), Old Faithful (60, 61), and Steamboat in Yellowstone (22), as well as for El Jefe in El Tatio, Chile (62). The height of the water column can vary from one eruption to another (e.g., refs. 18, 63); however, few studies (17, 63, 64) provide details about height measurements. Nevertheless, despite the unknown and possibly large uncertainties, there is a clear trend: Geysers with deeper water sources have taller eruptions (Fig. 9*B*).

To quantify how water-source depth Z_r affects eruption height h_j, we used a model for eruptions (*Thermodynamic and Mechanical Models for Eruptions*) in which the fluids in the water source expand isentropically during eruption, and mechanical work is converted into kinetic energy, gravitational potential energy, and other forms of mechanical energy (friction in the conduit and then drag on erupted fluids, fragmentation, and sound). The ballistic velocity (V_b in Eq. **M3**) is typically lower than the jet velocity (V_j in Eq. **M2**) because of drag on the jet from the surrounding air. Here, we adopted an estimate suggesting the ratio of 0.5 for the ballistic over jet velocities at Lone Star Geyser (63). Substituting Eq. **M3** into Eq. **M2** and rewriting E_d (forms of mechanical energy) as an efficiency term ($-(1-\zeta)W$), Eq. **M1** is rewritten in terms of the jet height h_j as a function of water source depth Z_r as

$$h_j = -\frac{1}{4}\left(\frac{\zeta W}{g} + Z_r\right), \qquad [1]$$

where ζ is a conversion factor of W (mechanical work) into the kinetic and potential energies which varies between zero and one (65), and g is gravitational acceleration.

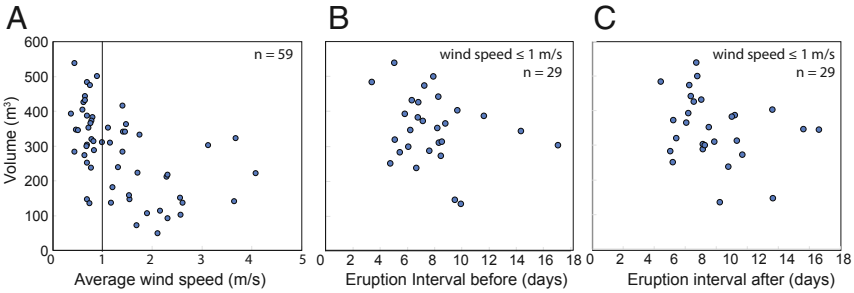

Fig. 8. (*A*) Volume of erupted water estimated from the Tantalus Creek streamgage and wind speed for 59 eruptions. This plot shows that lower volumes are related to higher wind speed. (*B*) Volume of erupted water and preceding interval for 29 eruptions occurring under low wind speed (≤1 m/s; line in *A* marks this threshold). (*C*) Volume of erupted water and interval after eruption for the same population as in *B*.

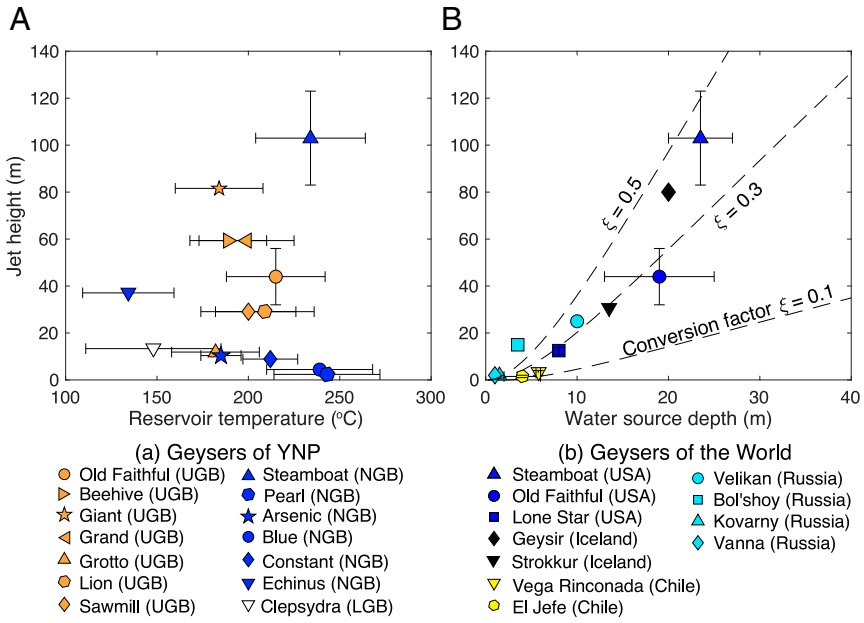

Fig. 9. (*A*) Jet height versus reservoir temperature of Yellowstone geysers in Upper Geyser Basin (UGB), Lower Geyser Basin (LGB), and Norris Geyser Basin (NGB). Data sources for water chemistry used with the iGeoT MEG code are detailed in *Geothermometry*; jet heights are from Bryan (18). (*B*) Thermodynamic model of jet height and water-source depth alongside real data. The dashed lines show predictions from Eq. **1** when ζ, a conversion factor of mechanical work into kinetic and potential energies, is varied. Data are from the following sources: Vanna, Kovarny, Bol'shoy, and Velikan (56); El Jefe (64); Vega Rinconada (49); Strokkur and Geysir (57); Steamboat (22); Old Faithful (60, 61); and Lone Star (58, 59, 63). Uncertainties are shown only if provided in the cited papers, and uncertainties in jet height are likely greater than 10%.

The dashed lines in Fig. 9*B* show the correlation between h_j and Z_r predicted by Eq. **1**. Data from geysers are mostly consistent with conversion factors of 0.3 to 0.5, similar to values suggested in Thiéry and Mercury (65). Our calculations suggest that the mechanical work of the mixture during expansion is correlated with water-saturation pressure. The kinetic energy at the vent and resulting jet height are, thus, expected to increase with water-source depth. Differences in eruption height at a single geyser could arise from the water initially being slightly oversaturated or undersaturated, variable friction loss, and external influences such as wind.

Our focus here has been on the eruption height, but we also note that Steamboat's erupted volume can exceed 500 m^3 (Fig. 8). Few geysers have estimates of erupted volumes because water discharge is challenging to measure, but those with estimates erupt less water: 8 to 11 m^3 during major eruptions at Lone Star (63); uncertain estimates of 38 to 45 m^3 (12) and 14 to 32 m^3 for Old Faithful (ref. 66, based on ref. 53); 31 to 38 m^3 for Echinus in Norris Geyser Basin (67); 18 m^3 for Velikan in Kamchatka, Russia (68); and 10^{-1} m^3 for El Jefe in El Tatio, Chile (64). Although individual Steamboat eruptions are large, the eruption intervals are relatively long and many other geysers erupt more water when averaged over time. Lone Star, for example, has been erupting about twice as much water annually than Steamboat during the current active phase (discounting preplay and minor eruptions for both geysers).

Concluding Remarks

Our study of Steamboat Geyser was motivated by three fundamental questions about geyser eruptions.

Why Did Steamboat Geyser Become Active Again? There are conflicting observations. Steamboat's reactivation was preceded by regional uplift and a slight increase in the median radiant temperature of Norris Geyser Basin. Whether this is coincidental or causal cannot be determined because we cannot establish this connection over multiple active phases. Despite the increase in thermal radiance, there was no significant change in the geothermal reservoir temperature, no increase in chloride and sulfate flux, and no evidence that other geysers became active in response to deformation. It is possible that dormant–active transitions in geysers may be controlled by gradual changes in silica precipitation that affect permeability in the geyser's subsurface. However, we acknowledge that direct observations of subsurface processes are lacking. Longer, continuous digital records of many observables will help identify possible connections between deformation, magmatic processes, and the surface expression of geothermal systems in the form of geyser eruptions.

What Controls the Interval between Eruptions? Based on 2.4 y of data, there is evidence for a small seasonal modulation of eruption intervals, with shorter intervals in the summer. This might suggest that intervals are modulated by the seasonal hydrologic cycle. Anomalously long intervals are associated with decreases in seismic noise measured at a nearby seismometer. We are unable to identify any relations between eruption intervals and erupted volumes, implying unsteady heat and mass discharge. Our volume estimates are hampered by relying on a streamgage well downstream from the vent and the fact that the site may not capture all erupted water, especially on windy days. A lack of reliable water-discharge measurements is the case for most geysers.

Why Are Steamboat's Eruptions Taller Than at Other Geysers? Steamboat's erupted water is stored deeper than at other geysers. If eruptions begin when water is at the saturation temperature, water in deeper sources has more thermal energy that can be converted to mechanical work and kinetic energy driving the eruption. We found a correlation between the depth of the shallow-water sources (bubble traps) under geysers and eruption height, but we highlight that there is much uncertainty in estimating source depth and eruption height.

To address these three questions, we relied heavily on monitoring data and observations. Few geysers are monitored well enough to have a continuous record of eruption times, water discharge, or geophysical data. To the extent that the questions motivating our study are interesting and worth answering, at least for the millions of tourists who visit Yellowstone each year, more instrumentation is required in and around geysers. Measuring ground-surface displacements, water discharge closer to the vent, and meteorological conditions, in addition to more frequent water sampling for chemical and isotopic analyses, would be useful to reduce uncertainty in observations. Such data would help answer fundamental questions about how geysers

work and provide insight into similar multiphase processes and associated geophysical signals that occur at volcanoes (53) and on other planetary bodies, such as Saturn's moon Enceladus (69).

Methods

Eruption Datasets. Eruption data were obtained from GeyserTimes (https://www.geysertimes.org/retrieve.php), a crowdsourced database of eruption times and observations compiled by geyser enthusiasts. We retrieved primary entries for Steamboat eruptions to generate the counts plotted in Fig. 2. Start times from the late-2010s active phase are exact and based on visual reports combined with seismic and temperature monitoring. The count of Steamboat eruptions in GeyserTimes is complete from May 1982 onward; prior to this, entries are based on memos, reports, and logbooks in the Yellowstone National Park archives. The majority of events were recorded because eruptions are conspicuous and can be inferred from posteruptive activity. At the time of this study, the GeyserTimes dataset contained 85 eruptions for the 1960s, which is less than the 104 reported in yearly counts by White et al. (2). This discrepancy is due in part to the requirement that GeyserTimes entries must be associated with a date, which leaves out eruptions that were reported or inferred within any period longer than a few days and eruptions for which conflicting dates appear in different sources. Entries are added or updated upon discovery of new historical records.

We also examined the timing of active and dormant periods for other Yellowstone geysers since 1990 to compare with caldera deformation: Ledge in Norris Geyser Basin; King and Hillside in West Thumb Geyser Basin; Fan and Mortar, Giantess, Giant, and Splendid in Upper Geyser Basin; and Black Diamond in Biscuit Basin (*SI Appendix*, Fig. S5). Their records are based on visual reports and, when available, temperature loggers in runoff channels. Because these geysers are large and/or rarely active, they generate interest in the Yellowstone geyser-enthusiast community and are, therefore, reported consistently. We checked completeness by cross-referencing the GeyserTimes datasets with Bryan (18), logbooks from the Old Faithful Visitor Center (observations of geyser activity from National Park Service staff and volunteers; transcribed at https://www.gosa.org/ofvclogs.aspx), and reports published in the Geyser Observation and Study Association newsletter. Despite suffering from some reporting bias, these datasets capture the geysers' active and dormant periods well.

Seismicity. We acquired both local and teleseismic earthquake catalogs from the US Geological Survey (USGS) (https://earthquake.usgs.gov/earthquakes/search/) and the Incorporated Research Institutions for Seismology (IRIS) (ds.iris.edu/ieb). In particular, we searched for local earthquakes with magnitudes 0 to 4.8 occurring between January 2003 and July 2020 around the northern border of the Yellowstone Caldera, in a region delimited by coordinates (44.635°, −111.275°) to (44.785°, −110.19°) (Fig. 1). For teleseismic earthquakes, we searched for earthquakes occurring globally between January 2017 and July 2019 with magnitudes >5.5, yielding 741 distant events (over 1,000 km) and 2 regional events (~270 km) located in Montana.

At station YNM, located ~330 m from Steamboat (Fig. 1), we calculated the PGV produced by both the local and teleseismic earthquakes and searched for correlation with Steamboat's activity. PGV is a proxy for local ground motion produced by earthquakes and is positively correlated with changes in permeability that may influence hydrothermal flow (30). We first downloaded the continuous daily seismic data of station YNM in the Yellowstone National Park Seismograph Network from the IRIS MetaData Aggregator (ds.iris.edu/mda/WY/). The instrument response was removed to obtain the velocity record, and then we cut the local and teleseismic earthquake waveforms based on the event-origin time. The PGV for local earthquakes was evaluated for all frequencies, but the PGV for teleseismic earthquakes was calculated after applying a 1-Hz low-pass filter to focus on the low-frequency content of the dynamic stress and avoid the artifacts from the high-frequency energy at the site. Finally, we evaluated the three-dimensional PGV by taking the maximum value of the rms energy after combining all three components of ground motion.

We used continuous daily data segments from YNM to calculate the SSAM. For each day, we removed mean and trend, applied a Butterworth filter between 0.8 and 1.2 Hz, and cut the data into hourly segments. To avoid spurious seismic energy (e.g., earthquakes and anthropogenic activity), SSAM was calculated as the median amplitude of each hour and restricted to a window of 21:00 to 07:00 local time (Fig. 7 and *SI Appendix*, Fig. S6). The unit of SSAM is instrument count.

Ground Deformation. We obtained continuous ground-deformation measurements from the University of Nevada, Reno repository (geodesy.unr.edu/index.php; ref. 70). Data have been detrended and referenced to the North American plate. We focused on station NRWY (Fig. 1), located near Norris Geyser Basin, and data from other stations in Yellowstone can be found in *SI Appendix*, Fig. S5.

Thermal Emissions. We explored the long-term (years) variations of radiant heat emissions from the ground surface at Norris Geyser Basin. This analysis was performed through an automatic median-of-median algorithm that uses satellite-based thermal infrared data retrieved from MODIS. The method we used is an extension of the method presented in refs. 40, 71, and its fundamental components are summarized here.

We downloaded the MODIS radiance, geolocation, and cloud-mask products, covering the period 4 July 2002 though 15 March 2020, from NASA's Earth database repository (https://earthdata.nasa.gov/). In particular, we used the following products: MODIS Terra/Aqua Calibrated Radiances 5-Min Level-1B Swath 1km V006 (MOD021KM/MYD021KM), which provides accurate radiance values that are radiometrically calibrated and corrected for instrumental effects; MODIS Terra/Aqua Geolocation Fields 5-Min Level-1A Swath 1km V006 (MOD03/MYD03), which provides the geographical coordinates of the scenes; and MODIS Terra/Aqua Cloud Mask and Spectral Test Results 5-Min Level-2 Swath 1km V6.1 (MOD35/MYD35), which allows extraction of cloud-free pixels.

Scenes with less than ~10% cloud-free pixels in the 3,600 km^2 around Norris Geyser Basin were discarded to ensure a reliable statistical analysis, using only scenes that were minimally affected by clouds. For each of the remaining scenes, we extracted band 31 (10.780 to 11.280 μm) radiance data from cloud-free pixels and converted them to radiant temperature using Planck's function for simplicity. We then calculated the median radiant temperature in a 4-km^2 square region centered on Norris Geyser Basin (44.724°, −110.703°) and delimited by (44.706°, −110.728°) to (44.742°, −110.678°), as well as the median radiant temperature in a reference area outside Yellowstone National Park, a hollow rectangle with internal borders (45.625°, −111.969°) to (45.823°, −109.438°) and external borders (43.643°, −112.222°) to (45.805°, −109.184°). The analysis was performed with nighttime scenes only.

We calculated the difference between the median radiant temperature at Norris Geyser Basin and the median radiant temperature of the reference area. We then calculated the median value per day of that difference in order to produce a regular and continuous sampling rate of one sample per day that allowed for further signal processing. Gaps were filled by using the nearest interpolation method, and the resulting time series, which contains a seasonal component and noise, was low-pass-filtered through an iterative denoising technique consisting of a combination of wavelet and median filters (40). This denoising technique yielded the so-called median anomaly, which describes the long-term (years) variations of the median radiant temperature in a region of interest (here, Norris Geyser Basin) with respect to a reference area.

Hydrothermal Discharge. An estimated 98% of all hydrothermal discharge within Norris Geyser Basin is drained by Tantalus Creek (55), which begins from a source southeast of Echinus Geyser and flows north and northwest through the basin until reaching the Gibbon River (Fig. 1). The USGS operates streamgage 06036940 on Tantalus Creek, which records discharge measurements at 15-min intervals; there are select periods with 1- or 5-min interval gauge height data (all available from https://waterdata.usgs.gov/nwis). Signals of water discharge from Steamboat eruptions appear as pulses at the gauge that peak ~90 min after eruption initiation in 15-min interval data. To calculate the discharge from Steamboat's eruption, we handpicked signal start and end times, linearly interpolated baseflow between discharge measurements at the time picks, and then integrated the excess discharge over time (illustrated in *SI Appendix*, Fig. S9). From a population of 87 eruptions between 15 March 2018 and 6 March 2020 for which there were approved discharge data, 74 have discernable signals that were uncompromised by rainfall and could be used for volume calculations.

Meteorology, Hydrology, and Solute Flux. Weather conditions were measured with a LI-COR eddy covariance tower located ~1.5 km north of Steamboat Geyser. Measurements of air temperature, atmospheric pressure, and wind speed in three orthogonal directions at 10 Hz were averaged over 30 min (further details of instrumentation are in ref. 72; data are available from ref. 73). We took an average of the four values following the start of a Steamboat eruption for each parameter to correlate with calculated discharge. Meteorological data are available for most eruptions on and after 20 July 2018.

Following the method of Hurwitz et al. (28), discharges measured at two USGS streamgages were used as a proxy for precipitation. We took annual

data since 1960 from the Yellowstone River at Corwin Springs, Montana (streamgage 06191500). Though this location is 45 km north of Norris Geyser Basin (Fig. 1), it has a long-term, complete record, making it the best candidate for analysis. We also took monthly average discharge from the Gibbon River measured at Madison Junction (streamgage 06037100) for comparison against eruption intervals within the latest active phase. The Gibbon River flows adjacent to Norris Geyser Basin (hydrothermal discharge from Tantalus Creek flows into it), and the gauge is 15 km to the southwest (Fig. 1). Both datasets are available from https://waterdata.usgs.gov/nwis.

Chloride and sulfate concentrations in the Gibbon River, the majority of which originate from Norris Geyser Basin (41), are linearly related to specific conductance (74). We took specific conductivity measured at the streamgage (data available from ref. 75), converted to solute concentrations, and multiplied by water discharge to calculate flux.

Geothermometry. Geysers in Yellowstone usually erupt alkaline-chloride waters with high silica concentrations (76). Geothermometry based on the chemical composition of these waters provides estimates of the temperature at which the water equilibrated with a set of minerals, presumably in the deep geothermal reservoir. We calculated reservoir temperatures using the iGeoT MEG code (37). We used published geochemical data for Steamboat, Cistern Spring, and other geysers around Yellowstone: Arsenic, Blue, Pearl, Constant, and Echinus in Norris Geyser Basin; Clepsydra in Lower Geyser Basin; and Beehive, Giant, Grand, Grotto, Lion, Sawmill, and Old Faithful in Upper Geyser Basin (35, 77–83). In 2019, we collected four new water samples from Steamboat Geyser in a runoff channel ∼65 m from the South Vent (minor eruption discharge: 1 June and 15 July; major eruption discharge: 1 June and 18 July) and two samples directly from Cistern Spring (30 May and 15 July). Water chemistry for these samples is summarized in *SI Appendix*, Table S2. The selection of samples was based on the quality of the geochemical data and ionic imbalance <3%. For the iGeoT simulations, we assumed that the dry gas was 100% CO_2. We considered a common assemblage of hydrothermal (secondary) minerals based on borehole descriptions in Yellowstone, particularly borehole Y9 which is ∼400 m northeast of Steamboat (Fig. 1): quartz, chalcedony, cristobalite, chlorite, goethite, and different amounts of clays and iron oxides (2).

Thermodynamic and Mechanical Model for Eruptions. To understand the controls of eruption height, we used a model for the thermodynamics and mechanics of eruptions by considering the energy balance of the liquid and steam mixture during a geyser eruption. We assumed that water was initially in the saturated liquid state at a pressure equivalent to the hydrostatic pressure of the water source (63). Decompression as water ascends to the surface drives formation of steam bubbles, which are compressible and expand during ascent. The mechanical work, W, associated with decompression and steam expansion, is given by Thiéry and Mercury (65)

$$W = H_r - H_s, \quad \text{[M1]}$$

where H is the enthalpy of the mixture of water and steam, and subscripts r and s refer to the reservoir (water source) and ground surface, respectively. H is estimated from thermodynamic properties of water and steam (84), assuming the mixture expands isentropically. This assumption is justified because the ascent velocity of the mixture is high enough that heat transfer between water and the surrounding wall rock and from the escape of bubbles are negligible (63, 85). The mechanical work is converted into kinetic energy, gravitational potential energy, and other forms of mechanical energy (friction in the conduit and then drag on erupted fluids, fragmentation, and sound), E_d. Assuming the fluid velocity in the reservoir is negligible, the energy balance is given by

$$-W = gZ_r + \frac{1}{2}V_j^2 + \Delta E_d, \quad \text{[M2]}$$

where g is gravitational acceleration, Z_r is the reservoir depth, and V_j is the jet velocity at the surface. The kinetic energy at the surface is converted into the jet's gravitational energy at its highest point. The ballistic height, h_j, of the jet is estimated from

$$h_j = \frac{V_b^2}{2g}, \quad \text{[M3]}$$

where V_b is the ballistic velocity at the surface.

Data Availability. All study data are included in the article and *SI Appendix*.

ACKNOWLEDGMENTS. We thank the 2019 Cooperative Institute for Dynamic Earth Research program for enabling this collaboration (NSF Grant EAR1135452). M. A. Bellingham provided extensive historical context for Steamboat. We thank GeyserTimes users, in particular, Carol and Bill Beverly, for their detailed entries. Water samples were collected under permit YELL-2019-SCI-8104 with help from Yellowstone National Park research coordinator Annie Carlson; Xiaojing "Ruby" Fu, Matthew Kirk, and Nicole Mizrahi provided fieldwork assistance. Greg Vaughan, Jefferson Hungerford, and Blaine McCleskey added helpful input toward our analyses. We thank Einat Lev, Thomas Walter, and Mike Poland for constructive reviews. Additional support was provided by NSF Grant EAR1724986. Any use of trade, firm, or product names is for descriptive purposes only and does not imply endorsement by the US Government.

1. K. Flynn *et al., Database of the Geology and Thermal Activity of Norris Geyser Basin, Yellowstone National Park* (U.S. Geological Survey Data Series 324, U.S. Geological Survey, Reston, VA, 2008).
2. D. E. White, R. A. Hutchinson, T. E. C. Keith, "The geology and remarkable thermal activity of Norris Geyser Basin, Yellowstone National Park, Wyoming" (U.S. Geological Survey Professional Paper 1456, U.S. Geological Survey, Reston, VA, 1988).
3. L. A. Gastellum, *Description of Eruption of Steamboat Geyser as Observed by Luis A. Gastellum, Associate Superintendent December 25, 1962* (Geology Program Records (Box 82) (Yellowstone National Park Archives, Gardiner, MT, 1963).
4. S. Hurwitz, M. Manga, The fascinating and complex dynamics of geyser eruptions. *Annu. Rev. Earth Planet. Sci.* **45**, 31–59 (2017).
5. C. W. Wicks, D. Dzurisin, J. B. Lowenstern, J. Svarc, Magma intrusion and volatile ascent beneath Norris Geyser Basin, Yellowstone National Park. *J. Geophys. Res. Solid Earth* **125**, e2019JB018208 (2020).
6. R. O. Fournier, J. M. Thompson, C. G. Cunningham, R. A. Hutchinson, Conditions leading to a recent small hydrothermal explosion at Yellowstone National Park. *Geol. Soc. Am. Bull.* **103**, 1114–1120 (1991).
7. R. O. Fournier, Chemical geothermometers and mixing models for geothermal systems. *Geothermics* **5**, 41–50 (1977).
8. N. E. Matthews, J. A. Vazquez, A. T. Calvert, Age of the Lava Creek supereruption and magma chamber assembly at Yellowstone based on $^{40}Ar/^{39}Ar$ and U-Pb dating of sanidine and zircon crystals. *Geochem. Geophys. Geosyst.* **16**, 2508–2528 (2015).
9. R. L. Christiansen, "The Quaternary and Pliocene Yellowstone Plateau volcanic field of Wyoming, Idaho, and Montana" (U.S. Geological Survey Professional Paper 729-G, U.S. Geological Survey, Reston, VA, 2001).
10. J. Farrell, S. Husen, R. B. Smith, Earthquake swarm and b-value characterization of the Yellowstone volcano-tectonic system. *J. Volcanol. Geotherm. Res.* **188**, 260–276 (2009).
11. A. M. Pitt, C. S. Weaver, W. Spence, The Yellowstone Park earthquake of June 30, 1975. *Bull. Seismol. Soc. Am.* **69**, 187–205 (1979).
12. E. T. Allen, R. L. Day, *Hot Springs of the Yellowstone National Park* (Carnegie Institution of Washington, Washington, DC, 1935).
13. D. E. White, R. O. Fournier, L. J. P. Muffler, A. H. Truesdell, "Physical results of research drilling in thermal areas of Yellowstone National Park, Wyoming" (U.S. Geological Survey Professional Paper 892, U.S. Geological Survey, Reston, VA, 1975).
14. D. M. Churchill *et al*., Dating silica sinter (geyserite): A cautionary tale. *J. Volcanol. Geotherm. Res.* **402**, 106991 (2020).
15. S. Hurwitz *et al*., Yellowstone's Old Faithful Geyser shut down by a severe thirteenth century drought. *Geophys. Res. Lett.* **47**, e2020GL089871 (2020).
16. P. W. Norris, Report upon the Yellowstone National Park, to the Secretary of the Interior, for the Year 1879 (United States Government Printing Office, Washington, DC, 1880).
17. R. K. Schroeder, *Steamboat Geyser Eruption Heights* (Geology Program Records (Box 120) (Yellowstone National Park Archives, Gardiner, MT, 1963).
18. T. S. Bryan, *The Geysers of Yellowstone* (University Press of Colorado, Boulder, CO, ed. 5, 2018).
19. GeyserTimes, Eruptions of Steamboat Geyser, 1961–2020 and Ledge, Hillside, King, Black Diamond, Fan and Mortar, Splendid, Giant, and Giantess Geysers, 1990–2020 [online database]. https://www.geysertimes.org/retrieve.php. Accessed 1 August 2020.
20. F. D. Rentchler, *Steamboat Geyser Eruption*. Geology Program Records Box 120 (Yellowstone National Park Archives, Gardiner, MT, 1961).
21. M. Liesegang, C. T. Gee, Silica entry and accumulation in standing trees in a hot-spring environment: Cellular pathways, rapid pace and fossilization potential. *Paleontology* **63**, 651–660 (2020).
22. S.-M. Wu *et al*, Imaging the subsurface plumbing complex of Steamboat Geyser and Cistern Spring with hydrothermal tremor migration using seismic interferometry. https://doi.org/10.1002/essoar.10504609.1 (31 October 2020).
23. G. D. Marler, "Effects of the Hebgen Lake earthquake of August 17, 1959 on the hot springs of the Firehole geyser basins, Yellowstone National Park" in *The Hebgen Lake, Montana, Earthquake of August 17, 1959* (United States Government Printing Office, Washington, DC, 1964), pp. 185–198.
24. K. A. Barrick, Geyser decline and extinction in New Zealand: Energy development impacts and implications for environmental management. *Environ. Manage.* **39**, 783–805 (2007).

25. G. D. Marler, *What Do You Know about the Grand Geyser?* Geology Program Records Box 98 (Yellowstone National Park Archives, Gardiner, MT, 1962).
26. A. Gudmundsson, "Geysir" in *The Glorious Geology of Iceland's Golden Circle* (Springer, Cham, Switzerland, 2017), pp. 93–103.
27. S. Husen, R. Taylor, R. B. Smith, H. Heasler, Changes in geyser eruption behavior and remotely triggered seismicity in Yellowstone National Park produced by the 2002 M 7.9 Denali fault earthquake, Alaska. *Geology* **32**, 537–540 (2004).
28. S. Hurwitz, A. Kumar, R. Taylor, H. Heasler, Climate-induced variations of geyser periodicity in Yellowstone National Park, USA. *Geology* **36**, 451–454 (2008).
29. S. Hurwitz, R. A. Sohn, K. Luttrell, M. Manga, Triggering and modulation of geyser eruptions in Yellowstone National Park by earthquakes, earth tides, and weather. *J. Geophys. Res. Solid Earth* **119**, 1718–1737 (2014).
30. M. Manga *et al*., Changes in permeability caused by transient stresses: Field observations, experiments, and mechanisms. *Rev. Geophys.* **50**, RG2004 (2012).
31. C. H. Mohr, M. Manga, C.-Y. Wang, O. Korup, Regional changes in streamflow after a megathrust earthquake. *Earth Planet. Sci. Lett.* **458**, 418–428 (2017).
32. D. R. Shelly, J. L. Hardebeck, Illuminating faulting complexity of the 2017 Yellowstone Maple Creek earthquake swarm. *Geophys. Res. Lett.* **46**, 2544–2552 (2019).
33. G. Pang *et al*., The 2017–2018 Maple Creek earthquake sequence in Yellowstone National Park, USA. *Geophys. Res. Lett.* **46**, 4653–4663 (2019).
34. C. M. U. Neale, C. Jaworowski, H. Heasler, S. Sivarajan, A. Masih, Hydrothermal monitoring in Yellowstone National Park using airborne thermal infrared remote sensing. *Remote Sens. Environ.* **184**, 628–644 (2016).
35. H. Heasler, C. Jaworowski, Hydrothermal monitoring of Norris Geyser basin, Yellowstone National Park, USA, using airborne thermal infrared imagery. *Geothermics* **72**, 24–46 (2018).
36. R. G. Vaughan, L. P. Keszthelyi, J. B. Lowenstern, C. Jaworowski, H. Heasler, Use of ASTER and MODIS thermal infrared data to quantify heat flow and hydrothermal change at Yellowstone National Park. *J. Volcanol. Geotherm. Res.* **233–234**, 72–89 (2012).
37. N. Spycher *et al*., Integrated multicomponent solute geothermometry. *Geothermics* **51**, 113–123 (2014).
38. J. M. King *et al*., Multireaction equilibrium geothermometry: A sensitivity analysis using data from the Lower Geyser basin, Yellowstone National Park, USA. *J. Volcanol. Geotherm. Res.* **328**, 105–114 (2016).
39. R. O. Fournier *et al*., "Results of weekly chemical and isotopic monitoring of selected springs in Norris Geyser basin, Yellowstone National Park during June-September, 1995" (U.S. Geological Survey Open-File Report 2002-344, U.S. Geological Survey, Reston, VA, 2002).
40. T. Girona, V. Realmuto, P. Lundgren, Volcanoes show signs of large-scale thermal unrest for years prior to eruption. https://doi.org/10.1002/essoar.10503138.1 (12 August 2020).
41. R. B. McCleskey, D. K. Nordstrom, D. D. Susong, J. W. Ball, J. M. Holloway, Source and fate of inorganic solutes in the Gibbon River, Yellowstone National Park, Wyoming, USA: I. Low-flow discharge and major solute chemistry. *J. Volcanol. Geotherm. Res.* **193**, 189–202 (2010).
42. Yellowstone Volcano Observatory, "Yellowstone Volcano Observatory 2017 annual report" (U.S. Geological Survey Circular 1456, U.S. Geological Survey, Reston, VA, 2019).
43. S. E. Ingebritsen, S. A. Rojstaczer, Geyser periodicity and the response of geysers to deformation. *J. Geophys. Res. Solid Earth* **101**, 21891–21905 (1996).
44. R. O. Fournier, J. J. Rowe, The solubility of amorphous silica in water at high temperatures and high pressures. *Am. Mineral.* **62**, 1052–1056 (1977).
45. J. P. Icenhower, P. M. Dove, The dissolution kinetics of amorphous silica into sodium chloride solutions: Effects of temperature and ionic strength. *Geochim. Cosmochim. Acta* **64**, 4193–4203 (2000).
46. G. J. Weir, R. M. Young, P. N. McGavin, A simple model for Geyser flat, Whakaewerawera. *Geothermics* **21**, 281–304 (1992).
47. S. Rojstaczer, D. L. Galloway, S. E. Ingebritsen, D. M. Rubin, Variability in geyser eruptive timing and its causes: Yellowstone National Park. *Geophys. Res. Lett.* **30**, 1953 (2003).
48. G. D. Marler, Exchange of function as a cause of geyser irregularity. *Am. J. Sci.* **249**, 329–342 (1954).
49. C. Munoz-Saez, A. Namiki, M. Manga, Geyser eruption intervals and interactions: Examples from El Tatio, Atacama, Chile. *J. Geophys. Res. Solid Earth* **120**, 7490–7507 (2015).
50. S.-M. Wu *et al*., Anatomy of Old faithful from subsurface seismic imaging of the Yellowstone Upper Geyser basin. *Geophys. Res. Lett.* **44**, 10,240–10,247 (2017).
51. Yellowstone Volcano Observatory, Feeling perturbed: Seasonal disturbances of Yellowstone's hydrothermal systems. *Caldera Chronicles* (2018). https://www.usgs.gov/center-news/feeling-perturbed-seasonal-disturbances-yellowstones-hydrothermal-systems. Accessed 24 August 2020.
52. A. S. Shteinberg, An experimental study of geyser eruption periodicity. *Dokl. Phys.* **44**, 305–308 (1999).
53. S. W. Kieffer, Seismicity at Old Faithful Geyser: An isolated source of geothermal noise and possible analogue of volcanic seismicity. *J. Volcanol. Geotherm. Res.* **22**, 59–95 (1984).
54. E. P. Eibl *et al*, Eruption interval monitoring at Strokkur geyser, Iceland. *Geophys. Res. Lett.* **47**, e2019GL085266 (2020).
55. I. Friedman, "Monitoring changes in geothermal activity at Norris Geyser basin by satellite telemetry, Yellowstone National Park, Wyoming" in *Integrated Geoscience Studies in the Greater Yellowstone Area—Volcanic, Tectonic, and Hydrothermal Processes in the Yellowstone Geoecosystem*, L. A. Morgan, Ed. (U.S. Geological Survey Professional Paper 1717, U.S. Geological Survey, Reston, VA 2007).
56. A. Belousov, M. Belousova, A. Nechayev, Video observations inside conduits of erupting geysers in Kamchatka, Russia, and their geological framework: Implications for the geyser mechanism. *Geology* **41**, 387–390 (2013).
57. T. R. Walter *et al*., Underwater and drone based photogrammetry reveals structural control at Geysir geothermal field in Iceland. *J. Volcanol. Geotherm. Res.* **391**, 106282 (2018).
58. J. Vandemeulebrouck *et al*., Eruptions at Lone Star Geyser, Yellowstone National Park, USA: 2. Constraints on subsurface dynamics. *J. Geophys. Res. Solid Earth* **119**, 8688–8707 (2014).
59. A. Nayak *et al*, Origin and properties of hydrothermal tremor at Lone Star Geyser, Yellowstone National Park, USA. *J. Geophys. Res. Solid Earth* **125**, e2020JB019711 (2020).
60. J. Vandemeulebrouck, P. Roux, E. Cros, The plumbing of Old Faithful Geyser revealed by hydrothermal tremor. *Geophys. Res. Lett.* **40**, 1989–1993 (2013).
61. S.-M. Wu, F.-C. Lin, J. Farrell, A. Allam, Imaging the deep subsurface plumbing of Old Faithful geyser from low-frequency hydrothermal tremor migration. *Geophys. Res. Lett.* **46**, 7315–7322 (2019).
62. A. Ardid *et al*., Geometry of geyser plumbing inferred from ground deformation. *J. Geophys. Res. Solid Earth* **124**, 1072–1083 (2019).
63. L. Karlstrom *et al*., Eruptions at Lone Star Geyser, Yellowstone National Park, USA: 1. Energetics and eruption dynamics. *J. Geophys. Res. Solid Earth* **118**, 4047–4062 (2013).
64. C. Munoz-Saez *et al*., Dynamics within geyser conduits, and sensitivity to environmental perturbations: Insights from a periodic Geyser in the El Tatio geyser field, Atacama Desert, Chile. *J. Volcanol. Geotherm. Res.* **292**, 41–55 (2015).
65. R. Thiéry, L. Mercury, Explosive properties of water in volcanic and hydrothermal systems. *J. Geophys. Res.* **114**, B05205 (2009).
66. National Park Service, Old Faithful Geyser frequently asked questions (2018). https://www.nps.gov/yell/learn/nature/oldfaithfulgeyserfaq.htm. Accessed 13 September 2020.
67. L. E. Clor, J. B. Lowenstern, H. P. Heasler, "Systematics of water temperature and flow at Tantalus Creek during calendar year 2005, Norris Geyser Basin, Yellowstone National Park, Wyoming" (U.S. Geological Survey Scientific Investigations Report 2007-5234, U.S. Geological Survey, Reston, VA, 2007).
68. A. V. Kiryukhin, T. V. Rychkova, E. O. Dubinina, An analysis of hydrogeological behavior in the Geyser Valley, Kronotskii nature reserve, Kamchatka after the disaster of June 3, 2007. *J. Volcanol. Seismol.* **9**, 1–16 (2015).
69. C. C. Porco *et al*., Cassini observes the active south pole of Enceladus. *Science* **311**, 1393–1401 (2006).
70. G. Blewitt, W. C. Hammond, C. Kreemer, Harnessing the GPS data explosion for interdisciplinary science. *Eos*, 10.1029/2018EO104623 (2018).
71. P. Lundgren *et al*., The dynamics of large silicic systems from satellite remote sensing observations: The intriguing case of Domuyo volcano, Argentina. *Sci. Rep.* **10**, 11642 (2020).
72. J. L. Lewicki *et al*., Monitoring gas and heat emissions at Norris Geyser Basin, Yellowstone National Park, USA based on a combined eddy covariance and Multi-GAS approach. *J. Volcanol. Geotherm. Res.* **347**, 312–326 (2017).
73. J. L. Lewicki, L. M. Dobeck, Long-term gas and heat emissions measurements, Norris Geyser Basin, Yellowstone National Park. U.S. Geological Survey data release (2020). https://doi.org/10.5066/P9AKQFGV. Accessed 14 October 2020.
74. R. B. McCleskey *et al*., Solute and geothermal flux monitoring using electrical conductivity in the Madison, firehole, and Gibbon rivers, Yellowstone National Park. *Appl. Geochem.* **27**, 2370–2381 (2012).
75. R.B. McClesky *et al*, Specific conductance data for selected rivers and creeks in Yellowstone National Park, beginning in 2010 (version 2.0, May 2020). U.S. Geological Survey data release, https://doi.org/10.5066/F7BP011G (2019).
76. S. Hurwitz, A. G. Hunt, W. C. Evans, Temporal variations of geyser water chemistry in the Upper Geyser basin, Yellowstone National Park, USA. *Geochem. Geophys. Geosyst.* **13**, (2012).
77. J. M. Thompson, S. Yadav, "Chemical analyses of waters from geysers, hot springs and pools in Yellowstone National Park, Wyoming from 1974 to 1978" (U.S. Geological Survey Open-File Report 79-704, U.S. Geological Survey, Reston, VA, 1979).
78. J. M. Thompson, J. M. DeMonge, "Chemical analyses of hot springs, pools, and geysers from Yellowstone National Park, Wyoming, and vicinity, 1980-1993" (U.S. Geological Survey Open-File Report 96-98, U.S. Geological Survey, Reston, VA, 1996).
79. J. W. Ball *et al*., "Water-chemistry data for selected springs, geysers, and streams in Yellowstone National Park, Wyoming, 1999-2000" (U.S. Geological Survey Open-File Report 02-382, U.S. Geological Survey, Reston, VA, 2002).
80. R. B. McCleskey *et al*., "Water-chemistry data for selected springs, geysers, and streams in Yellowstone National Park Wyoming, 2001-2002" (U.S. Geological Survey Open-File Report 2004-1316, U.S. Geological Survey, Reston, VA, 2005).
81. J. W. Ball, R. B. McCleskey, D. K. Nordstrom, J. M. Holloway, "Water-chemistry data for selected springs, geysers, and streams in Yellowstone National Park, Wyoming, 2003-2005" (U.S. Geological Survey Open-File Report 2006-1339, U.S. Geological Survey, Reston, VA, 2006).
82. J. W. Ball, R. B. McCleskey, D. K. Nordstrom, "Water-chemistry data for selected springs, geysers, and streams in Yellowstone National Park, Wyoming, 2006–2008" (U.S. Geological Survey Open-File Report 2010-1192, U.S. Geological Survey, Reston, VA, 2010).
83. R. B. McCleskey *et al*., "Water-chemistry data for selected springs, geysers, and streams in Yellowstone National Park, Wyoming, beginning 2009" (U.S. Geological Survey Open-File Report 02-382, U.S. Geological Survey, Reston, VA, 2014).
84. W. Wagner *et al*., The IAPWS industrial formulation 1997 for the thermodynamic properties of water and steam. *J. Eng. Gas Turbine. Power* **122**, 150–184 (2000).
85. S. W. Kieffer, Sound speed in liquid-gas mixtures: Water-air and water-steam. *J. Geophys. Res.* **82**, 2895–2904 (1977).